ChemComm

Cite this: *Chem. Commun.*, 2011, **47**, 4252–4254

www.rsc.org/chemcomm

COMMUNICATION

In situ synthesis of MoS_2/graphene nanosheet composites with extraordinarily high electrochemical performance for lithium ion batteries†

Kun Chang and Weixiang Chen*

Received 1st February 2011, Accepted 17th February 2011
DOI: 10.1039/c1cc10631g

A facile process was developed to synthesize MoS_2/graphene nanosheet (GNS) composites by a one-step *in situ* solution-phase method. These MoS_2/GNS composites therefore exhibit extraordinary capacity, *i.e.*, up to 1300 mA h g^{-1}, and excellent rate capability and cycling stability as an anode material for lithium ion batteries.

The possibility of using a rechargeable lithium ion battery (LIB) for various stationary power storage applications has stimulated significant research activity aimed toward improving LIB energy, power density and cycling life. As a commercial anode material in LIBs, graphite suffers from a relatively small capacity (372 mA h g^{-1}) and should be replaced by alternative anode materials with higher capacity.[1] Recently, graphene, a flat one-atom-thick monolayer that is exfoliated from graphite, has been shown to exhibit outstanding electronic behavior, large surface area and high chemical tolerance, thus attracting much research interest.[2,3] These advantages suggest that graphene sheets hold promise as matrices for improving the electrochemical performance of metal and metal oxides.[4] To date, research concerning metal and metal oxides supported on graphene has greatly enhanced the electrochemical performance of graphene as an anode material for LIB.[5,6] Metal sulfides such as MoS_2, WS_2 and SnS_2 also deliver a higher theoretical capacity.[7]

As a typical layered transition metal sulfide, MoS_2 has a structure analogous to that of graphene. This metal sulfide is composed of three atom layers (S–Mo–S) stacked together through van der Waals interactions.[8,9] Due to this layered structure, Li^+ ions can easily intercalate and exfoliate. Since the patent publication of the first lithium ion battery using MoS_2 in 1980, several different MoS_2 morphologies have been used in lithium ion batteries.[10] Thus far, the highest specific capacity of MoS_2 was reported by Xiao *et al.* and is 1131 mA h g^{-1} with a current of 50 mA g^{-1}.[11] Because graphene has extraordinary electronic behavior, MoS_2 growth on the surface increases its electron conductivity and electrochemical performance.

Herein, we report a facile *in situ* solution-phase reduced method for growing MoS_2 layers on a graphene nanosheet (GNS) to form MoS_2/GNS composites. Electrochemical tests indicate that the MoS_2/GNS composites exhibit very high capacity and excellent rate capability and cycling stability as anode materials for LIB.

The *in situ* synthesis of MoS_2/GNS composites is shown schematically in Fig. 1a [also see ESI† for experimental details]. 0.035 g graphite powder was converted to graphene oxide (GO) by Hummers method.[12] The as-prepared GO was transferred from the as-made suspension into a 200 ml beaker with the addition of 40 ml DI water. Then, 0.3 g $Na_2MoO_4 \cdot 2H_2O$ was added. After ultrasonication and stirring for 20 min,

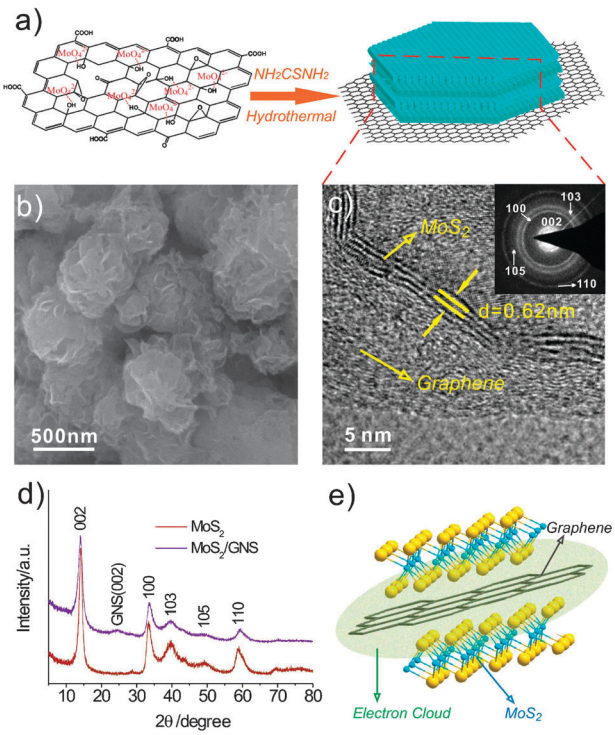

Fig. 1 (a) Schematic diagram of the *in situ* synthesis of MoS_2/GNS. (b) SEM image of MoS_2/GNS composites. (c) HRTEM image of MoS_2 layers on graphene. (d) XRD patterns of MoS_2 and MoS_2/GNS; inset shows the electron diffraction pattern of the MoS_2 nanosheets on graphene. (e) Schematic illustration of the microstructure of MoS_2/GNS.

Department of Chemistry, Zhejiang University, Hangzhou, PR China 310027. E-mail: weixiangchen@zju.edu.cn; Fax: +86 571-87951895; Tel: +86 571-87952477

† Electronic supplementary information (ESI) available: Experimental details and figure. See DOI: 10.1039/c1cc10631g

0.1 M NaOH was added to the solution until the pH value changed to 6.5. The mixture and 0.8 g NH_2CSNH_2 were dissolved in 80 ml DI water and then transferred into a 100 ml Teflon-lined stainless steel autoclave, sealed tightly, and heated at 240 °C for 24 h. After cooling naturally, the black precipitates were collected by centrifugation, washed with DI water and ethanol, and dried in a vacuum oven at 80 °C for 24 h. Due to the many functional groups on the surface of GO, such as carboxyl, hydroxyl and epoxy groups, as a result, MoO_4^{2-} anions could tightly adsorb onto the GO surface and then be reduced by NH_2CSNH_2 in the solution at 240 °C to form MoS_2/GNS composites. In this process, H_2S, which is released from NH_2CSNH_2 at high temperatures, reduces MoO_4^{2-} and GO to MoS_2 and graphene (see ESI†, Fig. S1). From the analysis of EDAX, four kinds of elements can be observed, *i.e.*, C, Mo, S and a small number of O, and it is calculated that the atomic ratio of Mo to C approaches to 1 : 2.

The general morphology of the MoS_2/GNS composites is shown in Fig. 1b. The composites deliver a 2-dimensional nanoflake structure. The high-resolution TEM (HRTEM) image shows that MoS_2 layers with an interlayer distance of 0.62 nm are grown on the surface of graphene (Fig. 1c). Comparing with the HRTEM image of pure MoS_2 (see ESI†, Fig. S1b), it can be found that the thickness of MoS_2 grown on the surface of graphene is about 4–5 layers, which is quite smaller than pure MoS_2 (tens of layers). This factor indicates that during the process of synthesis of MoS_2/GNS composites, MoS_2 is *in situ* reduced on the surface of graphene layers, and the graphene sheets greatly inhibit the restacking of MoS_2 layers. The same characteristic can be observed by XRD analysis (Fig. 1d). As shown in Fig. 1d, the MoS_2/GNS composite shows the similar crystalline structure of pure MoS_2, which are in good agreement with a hexagonal structure (JCPDS 37-1492). Additionally, the XRD patterns of the MoS_2 and MoS_2/GNS composites show that the growth of the (002) plane at $2\theta = 14.2°$ was inhibited due to the presence of graphene. The other diffraction peaks are in accordance with the electron diffraction pattern in Fig. 1c. A weak diffraction peak can be observed at $2\theta = 24.5°$, which is attributed to the (002) plane of graphene nanosheets (see ESI†, Fig. S1d). If only pure graphene sheets were reduced by H_2S in a hydrothermal process, it can be easy to restack for the graphene layers, and the interlayer distance of restacked graphene nanosheets is slightly large than that of graphite. Therefore, the increase of the interlayer of graphene nanosheets can provide larger space for Li ion intercalation, which also reduces the barriers to Li ion mobility, thereby facilitating lithium ion diffusion.[7a] In the composites, the electrons of the S atom layer and its adjacent carbon layer could form a co-electron cloud (Fig. 1e). The high concentration of electrons between the MoS_2 layer and the graphene layer could greatly enhance the electronic conductivity of the composites and were beneficial to the diffusion of the Li^+ ions during the charge and discharge in LIB.[13]

The MoS_2/GNS composites were mixed with carbon black and polyvinyldifluoride (PVDF) in a weight ratio of 80 : 10 : 10. The obtained slurry was spread on a copper foil with 14 mm in diameter and 0.02 mm in thickness, dried at 120 °C for 12 h under a vacuum atmosphere (−0.1 Mpa), and then pressed to form a working electrode with active material loading of 1.50 mg cm^{-2}. The electrochemical tests were performed in a two-electrode cell with a Li foil as the counter electrode and a 1.0 M $LiPF_6$ solution in a mixture of EC/DMC (1 : 1 in volume) as the electrolyte. Fig. 2c shows the first two charge and discharge curves of the MoS_2/GNS composites at a current density of 100 mA g^{-1} and cycled between 3.0 and 0.1 V *vs.* Li^+/Li. As shown in Fig. 2c, two potential plateaus at ~1.2 and ~0.6 V are observed for the composite electrode in the first discharge, which is in accordance with the findings for MoS_2 (Fig. 2a). The plateau at 1.2 V is indicative of the formation of Li_xMoS_2, and the plateau variation in the lithium intercalation is attributed to the different defect sites of MoS_2. The discharge plateau at 0.6 V can be attributed to a conversion reaction process, which first entails the *in situ* decomposition of MoS_2 into Mo particles embedded in a Li_2S matrix and then the formation of a gel-like polymeric layer resulting from electrochemically driven electrolyte degradation.[14] In the first charge (delithiation) process, two potential plateaus at about 1.7 and 2.3 V are displayed. This result can also be observed in the CV curves of the composites (Fig. 2b and d). During the second discharge, two inconspicuous potential plateaus at about 2.0 and 1.2 V, and the potential plateau observed at 0.6 V in the first discharge, disappeared, which is in accordance with the findings for MoS_2. The reversible formation of Li_2S at the nanoscale based on the reaction: $MoS_2 + 4Li \leftrightarrow Mo + 2Li_2S$, accompanying the redox of Mo nanoparticles and the reversible growth of the gel-like layer, should be the plausible reason for the reversible capacity and the sloping voltage regions in the subsequent cycles.[15] In addition, during the first charge/discharge process, the lithiation capacity of MoS_2/GNS composites is 2200 mA h g^{-1}, and the delithiation capacity reaches 1300 mA h g^{-1}, which is much higher than the capacity of free MoS_2 and GNS (see ESI†, Fig. S2)

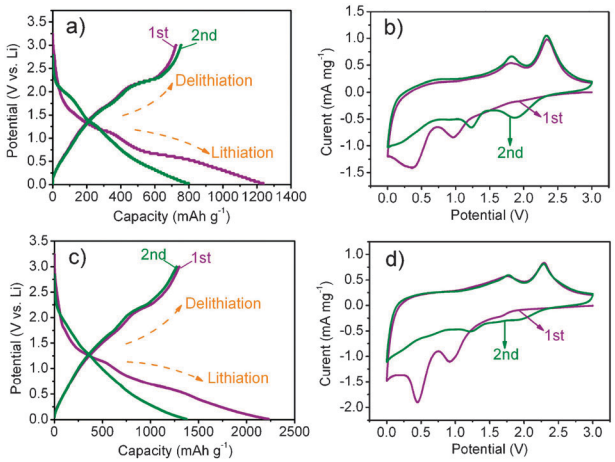

Fig. 2 Electrochemical characterizations of a half-cell composed of MoS_2 *vs.* Li and MoS_2/GNS *vs.* Li. (a) The first two charge and discharge curves of MoS_2 at a current density of 100 mA g^{-1}. (b) Cyclic voltammograms of MoS_2 electrodes at a scan rate of 0.5 mV s^{-1} during the first two cycles. (c) The first two charge and discharge curves of MoS_2/GNS at a current density of 100 mA g^{-1}. (d) Cyclic voltammograms of MoS_2/GNS electrodes at a scan rate of 0.5 mV s^{-1} during the first two cycles.

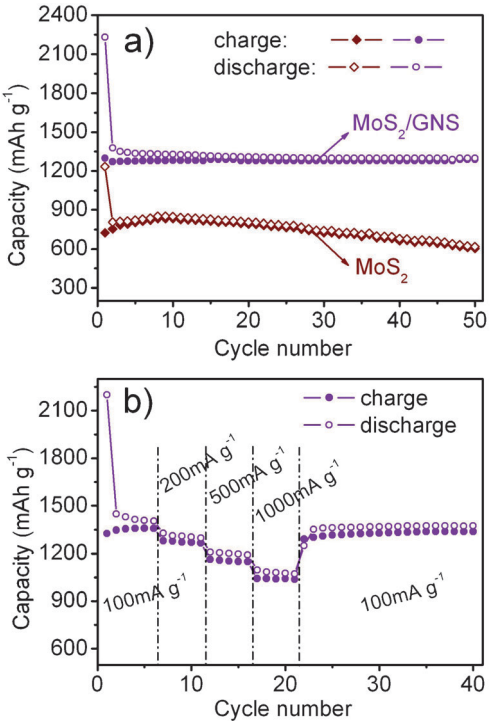

Fig. 3 (a) Cycling behaviors of MoS_2 and MoS_2/GNS at a current density of 100 mA g^{-1}. (b) Cycling behavior of MoS_2/GNS at various current densities.

obtained through the same method. As shown in Fig. 3a, MoS_2/GNS composites exhibit extraordinary cycling behavior and still retain the reversible capacity of 1290 mA h g^{-1} after 50 cycles. On the contrary, the reversible capacity of the free MoS_2 electrode reaches its maximum (835 mA h g^{-1}) after several cycles, but only a capacity of 605 mA h g^{-1} is retained after 50 cycles.

Such a high reversible capacity and excellent cycling behavior of the MoS_2/GNS composites are also exhibited in the rate capability. Fig. 3b shows the rate cycling behavior of the composites. The MoS_2/GNS composites also demonstrate good rate performance. Even at a high current density of 1000 mA g^{-1}, the specific capacity remains at 1040 mA h g^{-1}, which is still higher than that of free MoS_2 and GNS. Additionally, the extraordinary cycling stability of the composites is exhibited at various current densities. Even though the current changes from 1000 mA g^{-1} to 100 mA g^{-1}, the specific capacity of the composites returns to 1300 mA h g^{-1} at once and does not ultimately change in the following cycles, indicating extraordinarily high cycling stability. The high capacity, cycling stability and rate capability of the MoS_2/GNS composite could be attributed to the intimate interaction between the graphene substrates and MoS_2 layers grown on them, which was facilitated to MoS_2 electrochemically active since charge carriers could be effectively and rapidly conducted back and forth from MoS_2 layers to graphene layers.[5] In our experimental process, we found that the effect of the mole ratio of MoS_2 to GNS on the electrochemical performance of the composites was also important. Here, we reported a MoS_2/GNS composite with a Mo to C mole ratio of 1 : 2 that delivered the highest specific capacity ($\sim$1300 mA h g^{-1}). Although the specific capacity of samples with mole ratios of 1 : 1 and 1 : 4 (*i.e.*, 1001 mA h g-1 and 1132 mA h g-1, respectively) were inferior to that of a sample with a ratio of 1 : 2, these samples still exhibited higher specific capacity and better cycling stability than pure MoS2 and GNS (see ESI†, Fig. S3), indicating that initial electrochemical performances of MoS2 grown on the surface of graphene were indeed greatly enhanced and these kinds of MoS2/GNS composites would find wide applications as a promising anode material for LIB.

In summary, through the *in situ* reduction of MoS_2 nanoflakes on graphene nanosheets to form MoS_2/GNS composites, we enabled the MoS_2 anode material to achieve the highest specific capacity observed to date. The MoS_2/GNS composites can be further explored for high-capacity, low-capacity and environment-friendly anode materials for LIB applications. We believe that our facile method can also be used for other metal sulfides (*e.g.*, WS_2, SnS_2 and TiS_2) supported on graphene to significantly improve their electrochemical performances.

This work was supported by the Zhejiang Provincial Natural Science Foundation of China (Y407030, Y4100119) and 973 Fundamental Research Program from the Ministry of Science and Technology of China (2010CB635116).

Notes and references

1 M. Winter and R. J. Brodd, *Chem. Rev.*, 2004, **104**, 4245.
2 (*a*) A. K. Geim and K. S. Novoselov, *Nat. Mater.*, 2007, **6**, 183; (*b*) E. J. Yoo, J. Kim, E. Hosono, H. S. Zhou, T. Kudo and I. Honma, *Nano Lett.*, 2008, **8**, 2277; (*c*) B. Wang, X. L. Wu, C. Y. Shu, Y. G. Guo and C. R. Wang, *J. Mater. Chem.*, 2010, **20**, 10661.
3 (*a*) M. Pumera, *Chem. Rec.*, 2009, **9**, 211; (*b*) M. Pumera, *Energy Environ. Sci.*, 2011, DOI: 10.1039/C0EE00295J.
4 (*a*) Y. Li, W. Gao, L. Ci, C. Wang and P. M. Ajayan, *Carbon*, 2010, **48**, 1124; (*b*) H. L. Wang, H. S. Casalongue, Y. Y. Liang and H. J. Dai, *J. Am. Chem. Soc.*, 2010, **132**, 7472.
5 H. L. Wang, L. F. Cui, Y. Yang, H. S. Casalongue, J. T. Robinson, Y. Y. Liang, Y. Cui and H. J. Dai, *J. Am. Chem. Soc.*, 2010, **132**, 13978.
6 Z. S. Wu, W. Ren, L. Wen, L. Gao, J. Zhao, Z. Chen, G. Zhou, F. Li and H. M. Cheng, *ACS Nano*, 2010, **4**, 3187.
7 (*a*) G. Du, Z. P. Guo, S. Wang, R. Zeng, Z. Chen and H. Liu, *Chem. Commun.*, 2010, **46**, 1106; (*b*) J. W. Seo, Y. W. Jun, S. W. Park, H. Nah, T. Moon, B. Park, J. G. Kim, Y. J. Kim and J. Cheon, *Angew. Chem., Int. Ed.*, 2007, **46**, 8828; (*c*) J. W. Seo, J. T. Jang, S. W. Park, C. Kim, B. Park and J. Cheon, *Adv. Mater.*, 2008, **20**, 4269.
8 R. Tenne, L. Margulis, M. Genut and G. Hodes, *Nature*, 1992, **360**, 444.
9 H. S. S. Ramakrishna Matte, A. Gomathi, A. K. Manna, D. J. Late, R. Datta, S. K. Pati and C. N. R. Rao, *Angew. Chem., Int. Ed.*, 2010, **49**, 4059.
10 R. R. Haering, J. A. R. Stiles and K. Brandt, *US Patent*, 1980, No. 4224390.
11 J. Xiao, D. W. Choi, L. Cosimbescu, P. Koech, J. Liu and J. P. Lemmon, *Chem. Mater.*, 2010, **22**, 4522.
12 W. S. Hummers and R. E. Offeman, *J. Am. Chem. Soc.*, 1958, **80**, 1339.
13 C. R. German, P. Santiago, J. A. Ascencio, U. Pal, M. Perez-Alvarez, L. Rendon and D. Mendoza, *J. Phys. Chem. B*, 2005, **109**, 17488.
14 R. Dominko, D. Arcon, A. Mrzel, A. Zorko, P. Cevc, P. Venturini, M. Gaberscek, M. Remskar and D. Mihailovic, *Adv. Mater.*, 2002, **14**, 1531.
15 Q. Wang and J. H. Li, *J. Phys. Chem. C*, 2007, **111**, 1675.

